Novel experimental and 3D multiphysics computational framework for analyzing deformation and failure of composite laminates subjected to water blasts

Siddharth Avachat*, Min Zhou

The George W. Woodruff School of Mechanical Engineering, School of Materials Science and Engineering, Georgia Institute of Technology, Atlanta, GA 30332-0405, USA

ARTICLE INFO

ABSTRACT

The load-carrying capacity of composite structures under water-based impulsive loads is studied in relation to different materials and loading conditions. The analysis focuses on the role of fiber orientation, fiber stiffness and angle of structure obliquity relative to load direction on the deformation and failure in monolithic carbon-fiber and glass-fiber/epoxy composite plates of similar mass and thickness. Structures are subjected to impulsive loads of different intensities generated using the Underwater Shock Loading Simulator (USLS), a novel projectile-impact-based impulsive loading facility. In-situ high-speed digital imaging is used to study the deformation and failure, focusing on the effects of load intensity, failure modes and material heterogeneity. The experiments are combined with fully dynamic 3D Coupled Eulerian Lagrangian (CEL) finite element simulations accounting for the effects of fluid-structure interactions (FSI) and in-ply and inter-ply cracking and failure. It is found that the carbon-fiber laminates provide higher blast resistance, but transmit a greater fraction of the incident impulse to the supports than the glass-fiber laminates. Damage through in-ply and inter-ply cracking in the carbon-fiber laminates is ~25% of that in the glass-fiber laminates. Higher angles of load obliquity trigger localized deformation at multiple locations, leading to more extensive in-ply damage and progressively shear-dominated rupture.

© 2017 Elsevier Ltd. All rights reserved.

1. Introduction

The response of composite structures to both contact-induced dynamic and water-based impulsive loads is of great importance in the design of failure-resistant marine structures for naval and offshore industry applications in which composite materials have been increasingly employed. As a consequence, there is an increasing need to understand and quantify the response of composite structures to such high-intensity dynamic and impulsive loads. Chang and co-workers [1–3] have studied the damage behavior of composite laminates under low-velocity impact loading, concluding that in-ply matrix cracking precedes delamination growth and shear and bending crack initiation. The damage behavior of composite laminates is significantly influenced by matrix material, composite layup and geometric aspects such as size, thickness and loading area [4–6]. Minnaar and Zhou [7] used a novel interferometric experimental setup to show that interlaminar crack speeds are significantly higher under shear loading, and that crack speeds are strongly influenced by loading rate in mode II.

Experiments and computations focusing on different core topologies and specimen sizes have been carried out by Espinosa and co-workers [8–10]. Battley [11,12] developed and used a high-speed servo-hydraulic testing system and concluded that slamming impact on a deformable sandwich panels results in peak and residual pressures different from those for a rigid panels. Shukla and co-workers [13–17] examined the dynamic response of sandwich structures consisting of planar and curved composite structures. A combined experimental and computational analysis of deformation in composite structures subjected to underwater blasts carried out by Avachat and Zhou [18] has revealed that sandwich structures significantly outperform monolithic structures at all impulsive levels and environmental conditions including air-backed and water-backed conditions. Schiffer and Tagarielli [19, 20] analyzed the one-dimensional underwater blast performance of sandwich structures and showed that the impulse imparted to double hulls by underwater explosions can be dramatically reduced by employing the sandwich construction of the outer skin. They discovered a marked improvement in blast resistance in structures comprising a monolithic outer skin and an unsupported inner hull of similar mass in comparison to a stationary inner hull.

Despite the recent interest in the mechanical response of composite structures, especially their behavior under blast loading, there

* Corresponding author.
E-mail addresses: sidavachat@gatech.edu (S. Avachat), min.zhou@gatech.edu (M. Zhou).

are a number of unresolved issues. Comparative analyses of the blast resistance and dynamic performance of different reinforcements (glass-fiber, carbon-fiber), varying anisotropy, different matrix materials (epoxy, polyester, etc.), and varying loading conditions (planar, oblique, cylindrical) are lacking. The objective of the present study is to characterize the damage response of thick composite laminates with different reinforcements and anisotropies under water-based blast loading. The focus is on understanding the deformation and failure mechanisms and quantifying damage as a function of structural attributes, material properties, loading conditions and loading rates. Planar impulses resembling those resulting from underwater explosions are generated using the Underwater Shock Loading Simulator (USLS), a novel experimental setup developed recently. The USLS consists of a projectile-impact-based impulsive loading system, a water chamber, a target holder, and a safety enclosure.

Coupled Eulerian Lagrangian finite element simulations are carried out along with experiments, accounting for the experimental conditions and material properties which are measured independently. The simulations also account for the fluid-structure interaction (FSI) effect at the water-composite interface. Failure mechanisms considered include shear cracking and fragmentation, tensile cracking, compressive kinking, and interfacial debonding. The simulations focus on damage initiation and evolution in the early stage of deformation ($\sim$1500 μs) since the load-carrying capacity is most critically reflected then. This combined experimental and numerical approach enables the identification of factors that play important roles in determining the dynamic response of the materials. The analysis uses metrics such as deflection, transmitted impulse and accumulated damage to quantify the blast resistance.

2. Technical approach

2.1. Composites manufacturing

Fiber-matrix composites are composed of two distinct phases: (1) reinforcements like glass-fibers or carbon-fibers and (2) matrix materials like epoxy, polyester, etc. The strength and stiffness of the finished composite is determined by the volume fraction and directionality of fibers with respect to external loads. Two types of composite materials are used in this analysis: glass-fiber reinforced epoxy and carbon-fiber reinforced epoxy. The glass-fiber reinforced prepregs are 24-inch wide *XF0920/346-AA-675 E-Glass 300 GSM 36% RW. XF0920* is the resin designation, *346-AA-675* is the identification number of Owens Corning 346 Type 30 roving, *300 GSM* denotes the 300 g/m^2 areal mass of the aforementioned glass fiber, *675* denotes the length of the roving in yards per pound, and *36% RW* denotes resin weight in each lamina. The carbon-fiber reinforced prepregs are 24-inch wide *VTM 264/792/HTR40-300gsm 36% RW. VTM 264* is a variable temperature, vacuum processable epoxy resin developed by Cytec, *HTR40* is the identification number of Toho Tenax continuous fiber reinforcement, *300 GSM* denotes 300 g/m^2 areal mass of the aforementioned fiber reinforcement, and *36% RW* denotes resin weight in each lamina. The composite laminates are manufactured by curing the prepregs under pressure in a high temperature oven at 100 °C. The thickness of each cured lamina is calculated using

Cured Ply Thickness

$$= \frac{\text{Fiber Areal Weight}(\text{g} \cdot \text{m}^{-2})}{\text{Fiber density}(\text{g} \cdot \text{cm}^{-3}) \times \text{Fiber Volume}(\%) \times 10}, \quad (1)$$

giving a cured ply thickness of approximately 0.23 mm per layer or lamina. Each composite laminate is constructed by stacking unidirectional prepregs in the required orientations to create a dense, thick laminate with a total thickness of 6.5 mm. The layups studied in this analysis are bi-axial (0/90), quasi-isotropic (0/−45/45/90), unidirectional with fibers perpendicular to supports (90) and unidirectional with fibers parallel to supports (0). Fig. 1 shows the simply-supported planar impulsive loading configuration and the different layups used in laminate construction.

Marine vessels consist of geometrical nonlinearities like inclined and curved surfaces. Such sections interact with high intensity impulsive loads rather differently from the way planar sections do
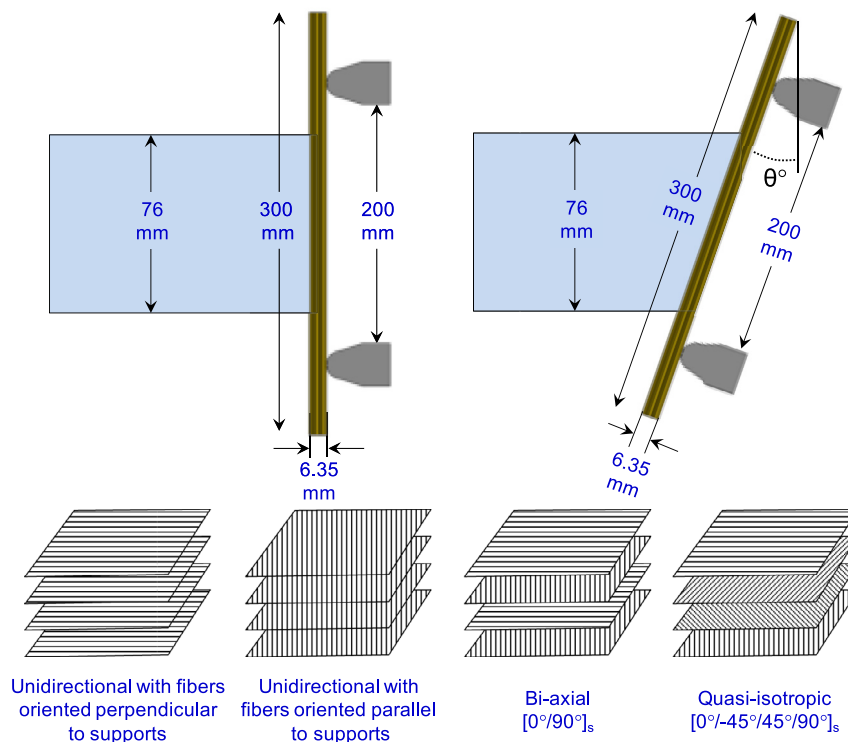
Fig. 1. Schematic illustration showing the simply-supported loading configuration with planar incident impulsive load and different composite layups of the test specimens.

under normal load incidence. The deformation and damage due to such geometric factors need to be considered for effective structure design. However, this aspect of underwater blast response has not been analyzed in the past. To evaluate the effects of load obliquity on the dynamic response of composite laminates, the loading angle is varied from 0° to 10° with increments of 2° and each configuration is subjected to similar incident loads. Fig. 1 illustrates such a loading configuration with a quasi-isotropic laminate.

2.2. Water-based impulsive loading experiments

Gas gun impact has been successfully used to generate impulsive loading through water [9,21−24]. To obtain controlled loading and simulate different water-structure contact conditions, the Underwater Shock Loading Simulator (USLS) in Fig. 2 is designed to provide a variety of loading configurations with quantitative diagnostics [21−23]. Important features of this facility include the ability to generate water-based impulsive loading of a wide range of intensity, the ability to simulate the loading of submerged structures, and integrated high-speed photographic and laser interferometric diagnostics. The impulsive load that impinges on the target induces deformation in the specimen at strain rates up to 10^4 s^{-1}. Projectile impact velocities in the range of 15−150 ms^{-1} are used to delineate the effect of loading rate on the deformation and failure behavior of the structures analyzed. This velocity range corresponds to peak pressures between 15 and 200 MPa, which are comparable to pressures observed in underwater explosions [25−28].

According to Taylor's analysis of one dimensional blast waves [29] impinging on a light, rigid, free standing plate, the pressure in the fluid at a distance r from an explosive source follows the relation $p(t) = p_0 \exp(-t/t_0)$, where p_0 is the peak pressure, t is time and t_0 is the pulse time on the order of milliseconds. The area under the pressure-time curve is the impulse carried by the wave and is given by $I_0 = \int p(t)\, dt = p_0 t_0$. For a free standing plate of areal mass m, the impulse transferred to the plate is $I_T/I_0 = \psi^{(\psi/1-\psi)}$, where $\psi = \rho_w c_w t_0/m$, and ρ_w is the density of water and c_w is the speed of sound in water. This FSI parameter is an important aspect

of Taylor's analysis because it helps to delineate the effects of a pressure pulse applied instantaneously versus the effects of a pressure pulse decaying over a certain time period. It has been shown that this FSI effect can be exploited to improve the blast mitigation capability of structures subjected to transient loads [30, 31].

2.3. Modeling of water-structure interaction

The model consists of a Lagrangian domain for composite materials and an Eulerian domain for water. In the Lagrangian domain, nodes are fixed within the material and nodal displacements track the material deformation. Since each Lagrangian element is always 100% within a single material, the material boundary coincides with element boundaries. In contrast, the Eulerian the domain consists of nodes that are fixed in space and the material flows through the elements that do not experience deformation. Eulerian elements may also be partially or completely void, allowing material to flow into empty space, capturing a crucial aspect of fluid flow. Materials tracked by Eulerian elements can interact with Lagrangian elements through Eulerian-Lagrangian contact algorithms to allow fully coupled multi-physics simulations like fluid-structure interactions. This Coupled Eulerian-Lagrangian (CEL) framework allows the severe deformation in water and the FSI to be captured. In addition to simulating the blast wave propagation in the USLS, the Eulerian formulation also captures the exponentially decaying pressure waves and resulting cavitation at the fluid-structure interface. The interaction between the water and structure is effected by coupling the nodes in the water to the corresponding nodes of the structure, thereby ensuring continuity of displacements when contact occurs.

The response of water in the Eulerian domain is described by the Mie-Grüneisen equation of state

$$p = \frac{\rho_0 c_0^2 \eta}{(1-s\eta)^2}\left(1 - \frac{\Gamma_0 \eta}{2}\right) + \Gamma_0 \rho_0 E_m, \qquad (2)$$

where p is pressure, c_0 is the speed of sound, ρ_0 is initial density, E_m is internal energy per unit mass, Γ_0 is Grüneisen's Gamma at a reference state, $s = dU_s/dU_p$ is the Hugoniot slope coefficient, U_s is the
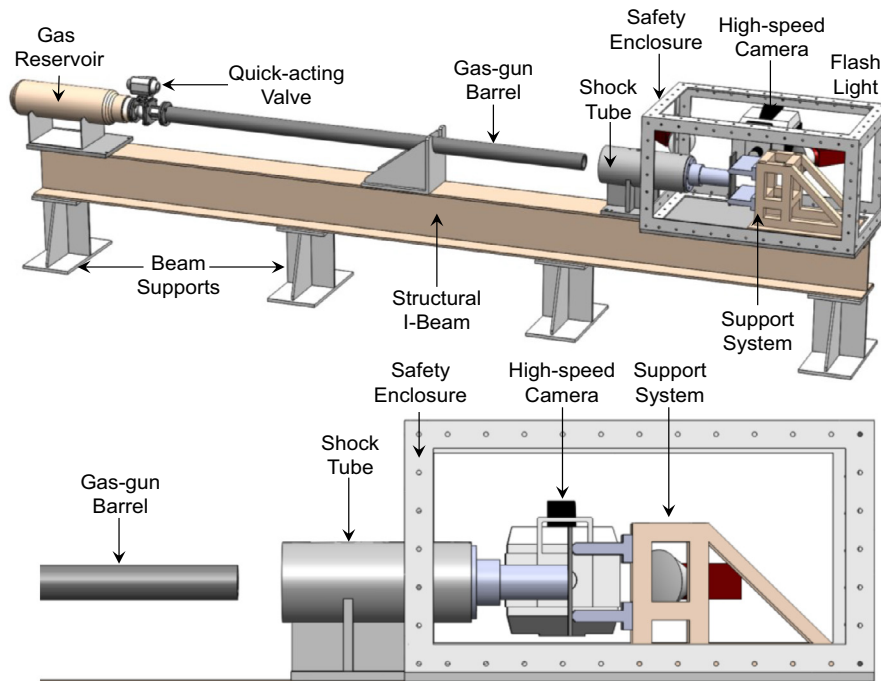
Fig. 2. Schematic illustration of the Underwater Shock Loading Simulator (USLS) for testing simply-supported thick laminates. Pictured are the gas reservoir, gun barrel, water chamber, modular support system, specimen and the Imacon 200D high-speed camera.

shock wave velocity, and U_p is particle velocity which is related to U_s through a linear Hugoniot relation

$$U_S = c_0 + sU_p. \tag{3}$$

The parameters for the Mie-Grüneisen equation of state are listed in Table 1. The space enclosed by the shock-tube is prescribed the properties of water while the space that is outside the shock-tube is kept as a "void", allowing water to flow into it as a result of high-pressure wave impinging on the target. This has the effect of instantaneously relieving the pressure in the water-chamber in a manner consistent with experimental observations. In the case of specimen rupture, the CL framework allows water to flow out of the breached portion.

2.4. Modeling of in-ply cracking and failure

Based on the energy required for initiation, matrix damage through cracking occurs first, followed by combined fiber-matrix debonding or "fiber-pullout" and finally fiber fracture. Damage occurring in the facesheets is accounted for using an energy-based damage evolution law [32] and [33]. The models assume a transversely isotropic solid which is perfectly elastic until the onset of damage. After damage initiation, following damage modes are accounted for through the simulatons: (1) matrix tension; (2) matrix compression; (3) fiber tension; and (4) fiber compression. The parameters used in these calculations can be found in [34] and [35]. In the simulations, a material-point has an initial, undamaged value of 1 and as the material-point experiences damage, this value decreases. The lowest value, before the material-point is removed from the simulation, is 0. The material properties of glass-fiber reinforced epoxy and carbon-fiber reinforced epoxy are provided in Tables 2 and 3 [36,37], respectively.

To alleviate mesh dependency during material softening, Abaqus introduces a characteristic length into the formulation, so that the constitutive law is expressed as a stress-displacement relation. The characteristic length, L_C, is based on the element geometry and formulation: it is a typical length of a line across an element for a first-order element. The damage variable will evolve such that the stress-displacement behaves as shown in each of the four failure modes. The positive slope of the stress-displacement curve prior to damage initiation corresponds to linear elastic material behavior; the negative slope after damage initiation is achieved by evolution of the respective damage variables according to the equations shown below. For each failure mode the energy dissipated due to failure, which corresponds to the area of the triangle OAC, must be specified.

2.4. Modeling of interfacial effects using cohesive elements

In the simulations, each unidirectional lamina is simulated explicitly to accurately represent the structure and behavior of the entire carbon-fiber/epoxy laminate and capture damage and deformation. The epoxy layers between two laminas, also called "resin rich layers", are modeled using cohesive elements to capture interfacial fracture and delamination. Due to the inherently heterogeneous nature of fiber-reinforced composites, interfacial separation plays a very important role in deformation. Interfacial separation of directionally stacked layers in the composite is called delamination. Delamination requires very little energy and is the dominant

Table 1
Parameters for the Mie-Gruneisen equation of state for water.

Parameter	Symbol	Unit	Value
Density of water	ρ	kg/m³	1000
Speed of sound in water	c	m/s	1482
Gruneisen's Gamma	Γ_0	–	0.1

Table 2
Material properties for unidirectional glass-fiber/epoxy laminates in [34].

Parameter	Symbol	Unit	Value
Density	ρ	kg·m⁻³	1850
Tensile modulus	E_{11}	MPa	39,000
Transverse modulus	E_{22}	MPa	9000
Shear modulus	G_{12}, G_{13}	MPa	3500
Longitudinal tensile strength	T_{11}	MPa	1200
Longitudinal compressive strength	C_{11}	MPa	900
Transverse tensile strength	T_{22}	MPa	45
Transverse compressive strength	C_{22}	MPa	128
Longitudinal shear strength	S_{12}, S_{21}	MPa	51
Transverse shear strength	S_{23}	MPa	51

Table 3
Material properties for unidirectional carbon-fiber/epoxy laminates [35].

Parameter	Symbol	Unit	Value
Density	ρ	kg·m⁻³	1580
Longitudinal tensile modulus	E_{11}	MPa	138,000
Transverse tensile modulus	E_{22}	MPa	10,000
Shear modulus	G_{12}, G_{13}	MPa	5240
Longitudinal tensile strength	T_{11}	MPa	2280
Longitudinal compressive strength	C_{11}	MPa	1440
Transverse tensile strength	T_{22}	MPa	57
Transverse compressive strength	C_{22}	MPa	228
Longitudinal shear strength	S_{12}, S_{21}	MPa	71
Transverse Shear strength	S_{23}	MPa	71

damage mode in composite materials subjected to impact or impulsive loads. It occurs primarily due to matrix failure and matrix-finer separation and reinforcing fibers are relatively intact. Similarly, core-facesheet separation is an important damage mode that occurs due to interfacial separation and fracture. If the bond between facesheet and core is weak, interfacial separation occurs. If the bond between the facesheet and the core is strong, tensile fracture in the foam leads to separation. Some commonly used metrics to evaluate the damage resistance of composites to impact loads are impact energy, displacement, delamination-area and extent of rupture.

The cohesive finite element method (CFEM) has been extensively used to study a wide variety of issues related to delamination and fracture such as tensile decohesion [39], quasi-static crack growth [40], ductile fracture [41, 42], dynamic fracture [43]), dynamic fragmentation [44], [45], delamination in composites [46], [47] and microstructural fracture [48]. Here, cohesive elements are specified at the interfaces between individual laminas in the composite structure as well as the interfaces between the aluminum and composite sections in the hybrid plates. The cohesive elements allow damage initiation and development in the interlaminar regions to be captured.
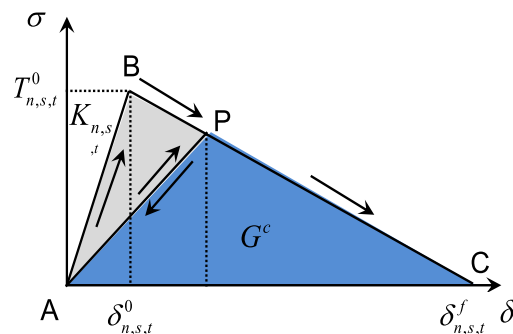
Fig. 3. Bi-linear law for cohesive traction-separation behavior.

Table 4
Material properties for epoxy [38].

Parameter	Symbol	Unit	Value
Normal stiffness	K_n	MPa	2000
Shear stiffness	K_s, K_t	MPa	2000
Critical normal traction	t_n^0	MPa	50
Critical shear traction	t_s^0, t_t^0	MPa	50
Critical normal fracture energy	G_n^C	N/mm	4.0
Critical shear fracture energy	G_s^C, G_t^C	N/mm	4.0

A bilinear traction-separation law shown in Fig. 3 is adopted to describe the behavior of the cohesive elements [46]. The parameters for all cohesive relations used are obtained from the work performed by Lapczyk and Hurtado [38] and are presented in

Table 4. The traction-separation stiffness for cohesive elements along interfaces between the laminas is 10^3 times the stiffness of the corresponding bulk elements. This choice has two benefits. First, artificial softening of the model is avoided. Second, the work of separation associated with the linear-elastic portion of the cohesive behavior is minimized, ensuring that the bulk of the work is in the fracture energy, providing adequate softening in the cohesive response. After failure of cohesive elements, contact between element faces is considered in the model using the a contact algorithm similar to that developed by Camacho and Ortiz [44]. If penetration is predicted, then penalty forces of sufficient magnitude are applied to the surfaces in the direction of their normal such that there is contact between them but minimum or no interpenetration.

The experimentally measured and calculated pressure pulses show good agreement in terms of peak pressures and decay times, as shown in Fig. 4. The experimentally measured profiles show slightly faster wave attenuation than the calculated profiles. Clearly, the coupled Eulerian-Lagrangian framework and the Mie-Gruneisen equation of state allow most essential features of the loading pulses in the experiments to be captured. Although the peak pressures are similar for experiments and simulations, the decay times are slightly different. The normalized impulse magnitude is $\bar{I} = 0.20$ for experiments and $\bar{I} = 0.16$ for simulations.

A laminate is discretized into two distinct interacting phases: (1) fiber-reinforced phase in the in-ply or intralaminar regions which are simulated using 3-D brick elements; and (2) resin-rich phase in the inter-ply or interlaminar regions which are simulated using cohesive finite elements of finite thickness. Failure is predicted when the damage operator in the respective case reaches unity. Once this rupture criterion is satisfied, the properties of failed elements are modified so that only compressive stresses are supported and tensile and shear stresses are eliminated. However, the predictions of damage and structural response based on such failure criteria are inherently mesh-size dependent as shown by Needleman and

Tvergaard [42] and Gullerud et al. [49]. When the stress-strain diagram exhibits a negative slope, the strain-softening damage tends to localize in a zone that is governed by element size. Since the damage dissipation per unit volume is finite, the vanishing damage zone causes the structure to fail at zero energy dissipation. In the current computational approach, the mesh size selection must ensure satisfactory strain resolution, realistic energy dissipation and must qualitatively reflect the experimentally observed deformation modes. To counteract this spurious mesh dependence associated with material softening, a characteristic element length L_E is introduced in ABAQUS. For 3-D elements, L_E is the cube-root of element volume. Following damage initiation, an equivalent displacement δ is introduced such that $\delta = L_E \cdot \varepsilon$ and evolves according to $\dot{\bar{\delta}} = L_E \cdot \dot{\bar{\varepsilon}}$ until it reaches a critical value. Although mesh refinement is essential for adequate strain resolution, excessive mesh refinement has the adverse effect of yielding anomalously low energy dissipation. As shown in Fig. 5, the numerical solution reaches convergence for a mesh width of $w = 500\,\mu$m. Consequently, the mesh width selected for this calculation is $w = 500\,\mu$m, which is sufficient for numerical convergence (in both, bulk and cohesive elements) but still provides a reasonable approximation of energy dissipated in the process. These element sizes are in accordance with element size recommendations from Tomar et al. [50] for cohesive elements.

3. Results and discussion

3.1. Experiments and validation of model

The deformation in a dynamically loaded composite laminate can be divided into two regimes: (1) flexural wave propagation towards the supports and (2) structural deflection. The flexural wave travels towards the supports in a very short time (~50 μs). Although the resolution of the camera is sufficient to capture this phenomenon, we are more interested in structural response in the form of damage and out-of-plane deflection, which take place over a longer time span. Consequently, the temporal resolution of the camera is selected to capture the behavior over a duration of 2 ms. The experiments and simulations are considered together in order to develop a detailed analysis and intimate understanding of structural failure in blast-loaded monolithic composite plates. Both quantitative and qualitative approaches are used to evaluate blast response.

In order to accurately compare the performance of composite structures under blast loading, we need to consider laminates of equal areal mass subjected to similar incident impulses. Since quasi-isotropic laminates are most widely used in commercial applications, we identified the incident failure impulse for a 6.35 mm thick quasi-isotropic laminate. A number of experiments were carried out to determine that the quasi-isotropic laminate fails under an impulsive load
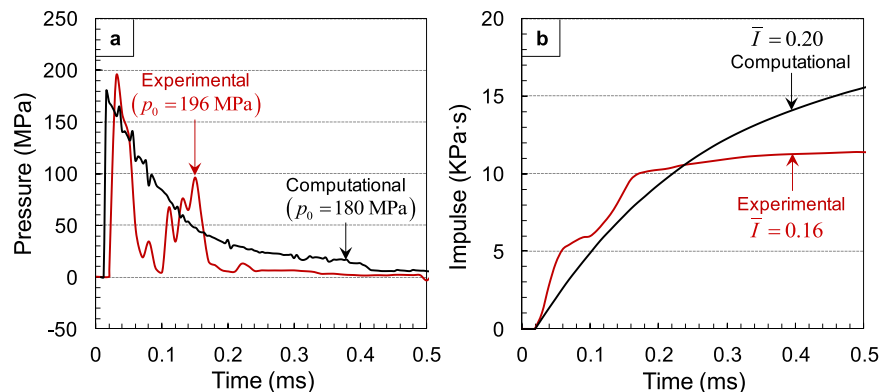
Fig. 4. Experimentally measured and numerically calculated pressure and impulse histories in the water chamber for a gas reservoir base pressure of 350 psi and a projectile velocity of ~110 ms^{-1}.
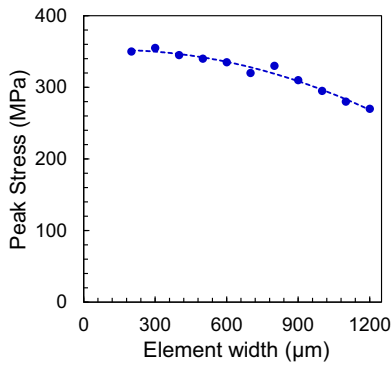
Fig. 5. Peak stress in the laminate as a function of element size for impulsively loaded composite laminates.

with a peak pressure of ~196 MPa. It was found that a gas reservoir base pressure of 350 psi generated an underwater pressure wave with a peak pressure of ~196 MPa with a variation of up to 20 MPa. Although the peak pressures are similar for experiments and simulations, the decay times are slightly different. The normalized impulse magnitude is $\bar{I} = 0.20$ for experiments and $\bar{I} = 0.16$ for simulations.

As discussed previously, the loading configuration consists of a simply supported composite beam which undergoes bending deformation. The magnitude and rate of bending is determined by the incident impulse. Fig. 6 shows a sequence of high-speed photographs showing the deformation in a monolithic carbon-fiber/epoxy composite laminate with a quasi-isotropic layup subjected to $\bar{I} = 0.08$. In this case, the composite laminate undergoes bending deformation, but the impulsive load is insufficient to cause failure. Since there is no failure, the water in the shock tube does not breach the laminate and instead, escapes the chamber by flowing sideways with respect to the composite, in the direction of high-speed camera.
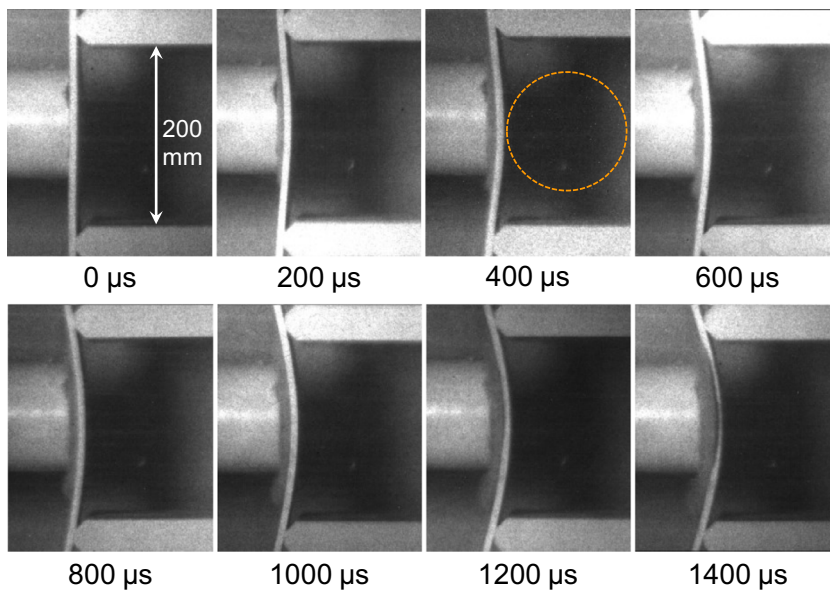
Fig. 6. Sequence of high-speed photographs showing the deformation in a monolithic carbon-fiber/epoxy composite plate with a quasi-isotropic layup subjected to $\bar{I} = 0.08$.
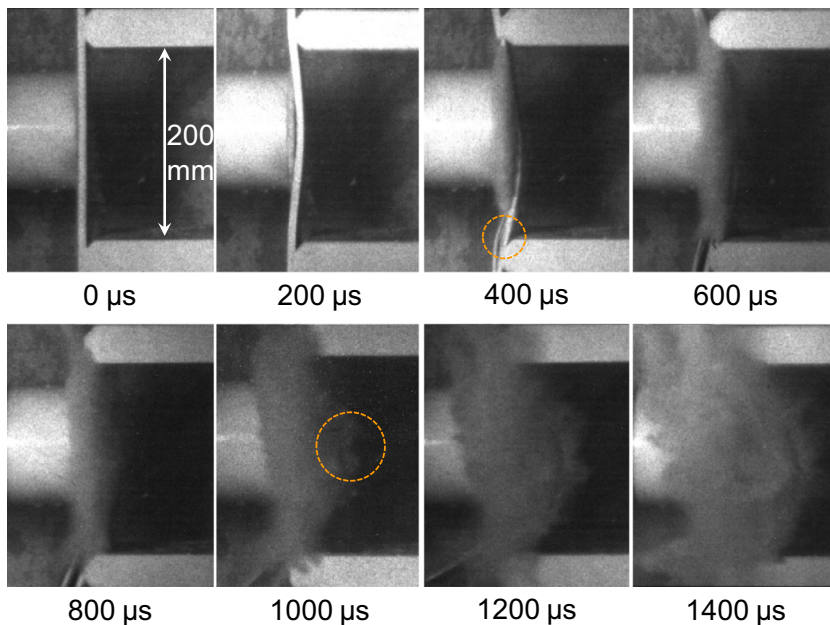
Fig. 7. Sequence of high-speed photographs showing the deformation in a monolithic carbon-fiber/epoxy composite laminate with a biaxial layup subjected to $\bar{I} = 0.16$.

Note the lack of any water in the space directly behind the composite as shown at $t = 400 \mu$s. Fig. 7 shows the sequence of high-speed photographs of deformation in a monolithic carbon-fiber/epoxy composite laminate with a biaxial layup subjected to $\bar{I} = 0.16$. A comparison of deformation at two different impulse magnitudes shows that at $\bar{I} = 0.16$. the pressurized water breaches the composite laminate and flows through the back side of the bending plate, clearly signifying rupture and catastrophic failure. In summary, tracking the behavior of the water column in touch with the specimen using high-speed digital imaging can provide an insight into the structural response, failure modes and collapse of each composite laminate.

Fig. 8 shows a sequence of high-speed photographs of a quasi-isotropic carbon-fiber/epoxy laminate subjected to $\bar{I} = 0.16$. Fig. 9

shows the in-ply damage contours for a quasi-isotropic carbon-fiber/epoxy laminate subjected to $\bar{I} = 0.20$. After the onset of bending deformation at $t = 200 \mu$s, the quasi-isotropic plate undergoes delamination near the midplane at $t = 400 \mu$s. The interlaminar cracks propagate towards the supports and cause further delamination near the edge at $t = 600 \mu$s. Since a simply-supported loading configuration causes maximum stresses near the midplane, a "hinge" or localized deformation develops in the laminate due to a combination of compressive and tensile stresses through the thickness. This observation is supported by the computational results shown in Fig. 9. It should be noted that although there is widespread delamination and in-ply damage, water flowing out of the shock tube does not breach the plate, instead flowing out of the sides as observed in Fig. 6. Results indicate that the computational
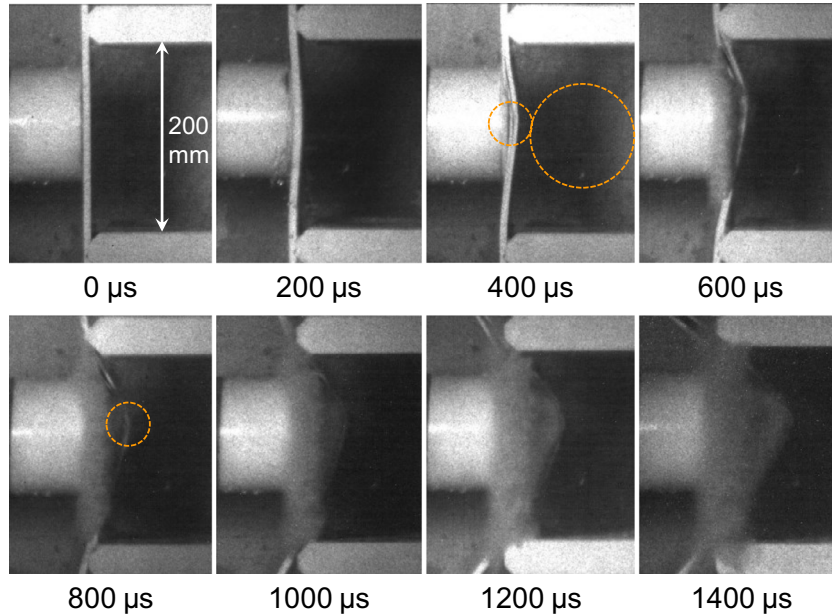
Fig. 8. Sequence of high-speed photographs showing the deformation in a monolithic carbon-fiber/epoxy composite plate with a quasi-isotropic layup subjected to $\bar{I} = 0.16$.
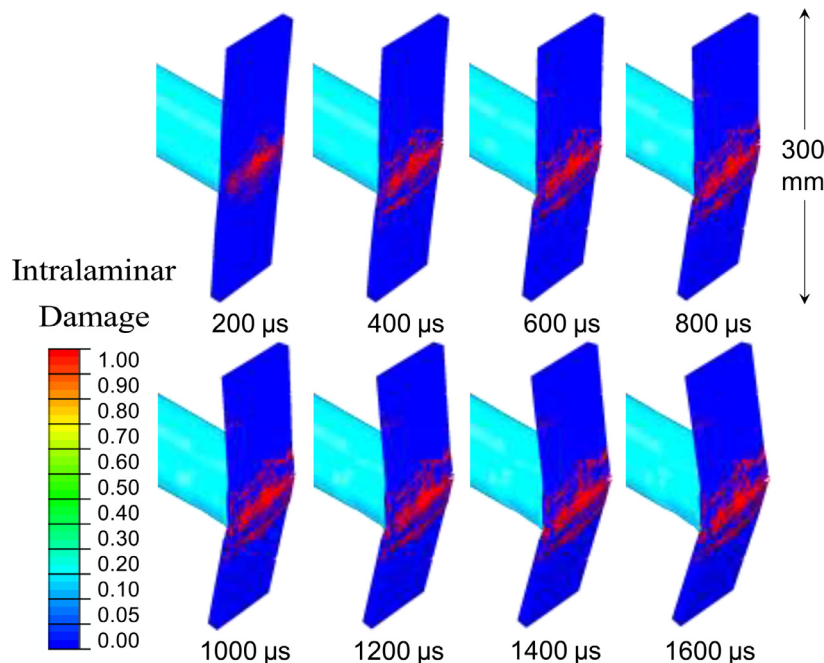
Fig. 9. Distributions of in-ply damage in quasi-isotropic carbon-fiber/epoxy composite laminate subjected to $\bar{I} = 0.20$.

model accurately captures the deformation observed in experiments.

As discussed previously, the quasi-isotropic layup exhibits large scale delamination but does not experience failure. In order to determine whether delamination can be localized to smaller region by modifying the laminate layup, laminates are constructed such that all laminas have fibers oriented parallel to the supports. Fig. 10 shows a sequence of high-speed photographs of a carbon-fiber/epoxy laminate with fibers oriented in a direction parallel to the supports subjected to underwater impulsive loads of similar magnitudes. After the onset of bending delamination at $t = 200$ μs, the plate experiences delamination at $t = 400$ μs. After delamination initiation, the delaminated sections of the laminate experience severe bending stresses leading to in-ply rupture at $t = 1000$ μs, followed by perforation of the plate near the midplane and catastrophic

failure at $t = 1200$ μs. The computational framework accounts for the effects of fiber orientation and captures the flow of water through the structure post-failure. Since the fibers are oriented parallel to the supports, a relatively smaller fraction of the incident impulse is transmitted to the supports leading significantly higher deflection and localized in-ply damage and fracture in close proximity to the impulsive wave loading area. Delamination is observed over a smaller area than the quasi-isotropic laminate, primarily near the loading region.

Fig. 11 shows a sequence of high-speed photographs of a carbon-fiber/epoxy laminate with fibers oriented in a direction perpendicular to the supports subjected to underwater impulsive loads of similar magnitudes. In this case, the plate is extremely stiff in the vertical direction and resists bending much more than the other layups. However, the lack of bending causes high shear stresses in the
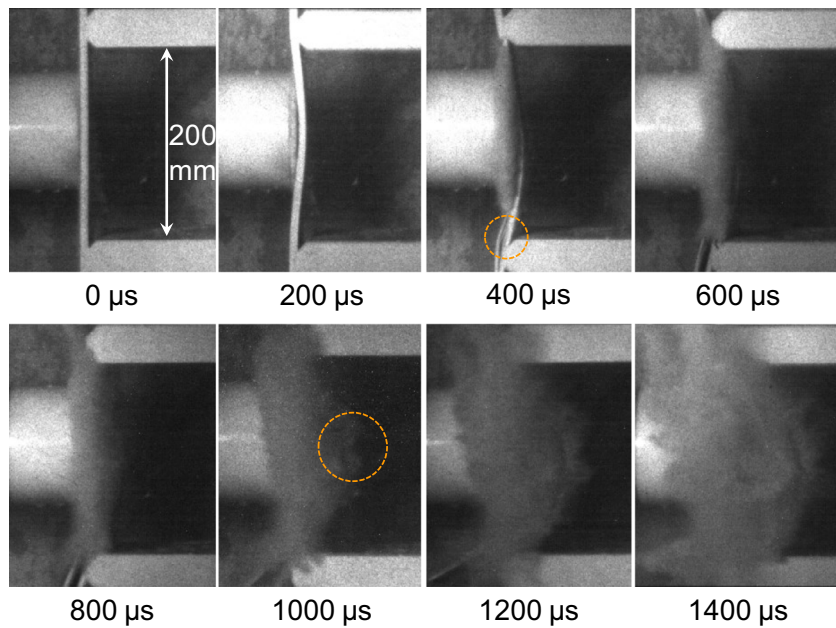
Fig. 10. Sequence of high-speed photographs showing the deformation in a monolithic carbon-fiber/epoxy composite laminate with fibers oriented parallel to the supports subjected to $\bar{I} = 0.16$.
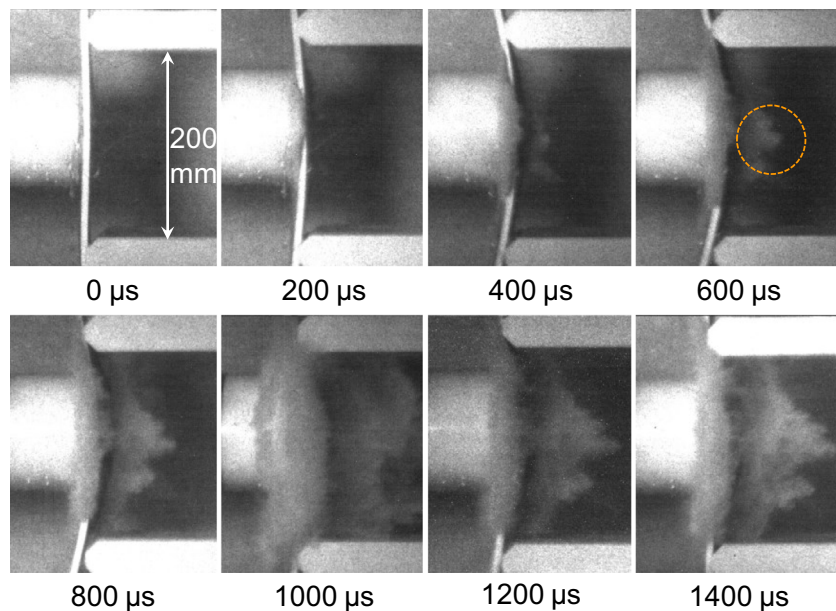
Fig. 11. Sequence of high-speed photographs showing the deformation in a monolithic carbon-fiber/epoxy composite laminate with fibers oriented perpendicular to the supports subjected to $\bar{I} = 0.16$.

laminate. Since the laminate lacks stability in the horizontal direction, the high transverse shear stresses cause "splitting" in the composite structure leading to failure at $t = 400 \ \mu s$. A comparison of the finite element simulations of the quasi-isotropic laminate with respect to the uniaxially oriented laminates reveals that the quasi-isotropic layup provides superior blat resistance by minimizing shear stresses in any particular region and distributing the incident impulsive load in a uniformly to avoid localized rupture.

Carbon-fiber/epoxy laminates exhibit exceptionally high stiffness and bending resistance due to the high elastic modulus of carbon fibers. Investigation of the underwater blast resistance of such laminates indicates that the composite plates are quite stable and blast resistant prior to damage initiation. However, after damage initiates, the laminates experience a dramatic loss in stiffness and undergo catastrophic failure and collapse. Additionally, carbon-fiber/epoxy laminates significantly more expensive in comparison to glass-fiber/epoxy laminates. With respect to the materials studied here and reported in this analysis, the carbon-fiber/epoxy laminates have a

unit cost that is more than twice as much as that of glass-fiber/epoxy laminates. Since marine structures often require large quantities of composite materials, cost considerations can play a major role in materials selection. To evaluate the differences in structural response of carbon-fiber and glass-fiber/epoxy laminates, a set of experiments and simulations is carried consisting of glass-fiber/epoxy laminates with different fiber layups subjected to incident impulses similar to those for the carbon-fiber/epoxy laminates. For brevity, high-speed photographs of all layups and computational results for only the quasi-isotropic layup are reported. The high-speed photographs are followed by a quantitative analysis of the blast response of both carbon-fiber and glass-fiber/epoxy laminates.

Fig. 12 shows a sequence of high-speed photographs of a biaxially oriented glass-fiber/epoxy laminate subjected to $\bar{I} = 0.16$. After the onset of bending at $t = 200 \ \mu s$, an in-ply crack initiates at the backface and propagates towards the frontface at $t = 600 \ \mu s$. This propagating crack deflects into two interlaminar cracks at $t = 800 \ \mu s$. The composite laminate loses stiffness and undergoes catastrophic
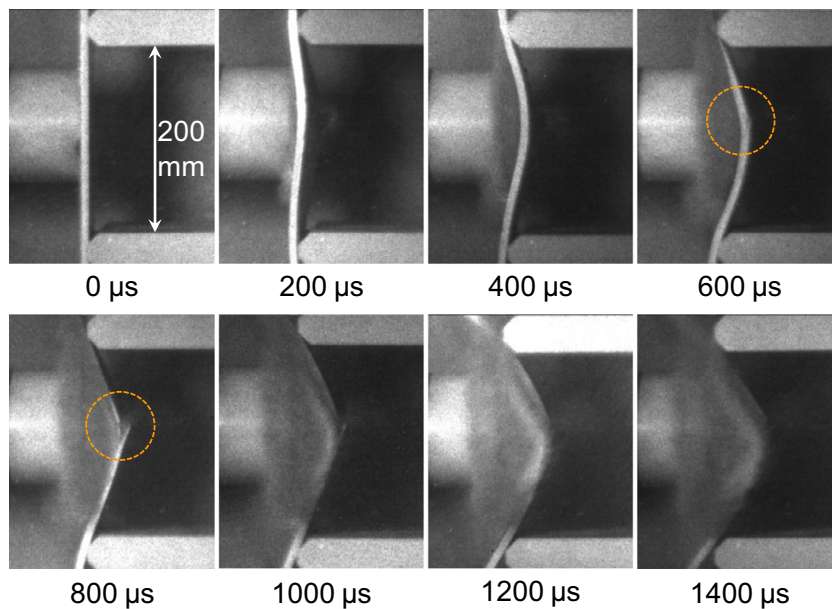
Fig. 12. Sequence of high-speed photographs showing the deformation in a monolithic glass-fiber/epoxy composite laminate with a biaxial layup subjected to $\bar{I} = 0.16$.
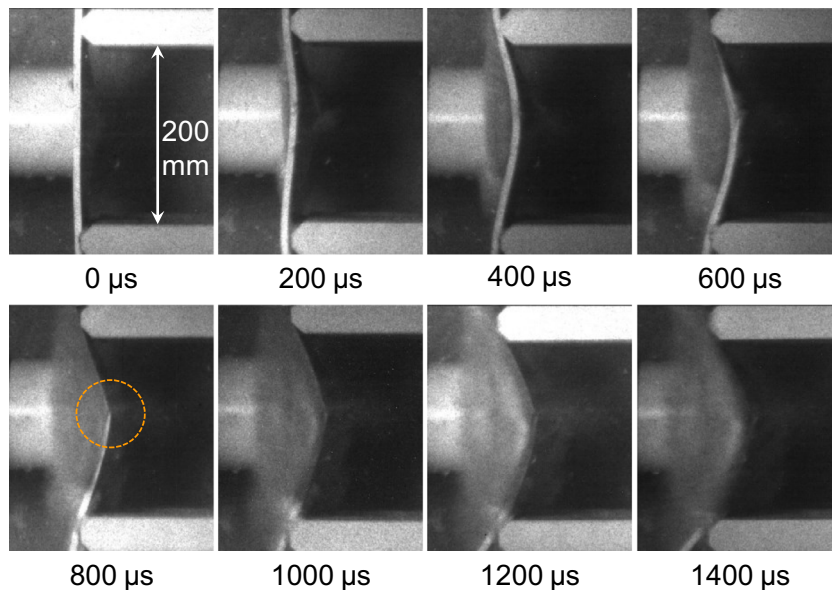
Fig. 13. Sequence of high-speed photographs showing the deformation in a monolithic glass-fiber/epoxy composite laminate with a quasi-isotropic layup subjected to $\bar{I} = 0.16$.

failure at $t = 1200$ μs. Fig. 13 shows a sequence of high-speed photographs of a quasi-isotropic glass-fiber/epoxy laminate subjected to $\bar{I} = 0.16$. Fig. 14 shows the in-ply damage contours for a quasi-isotropic glass-fiber/epoxy laminate subjected to $\bar{I} = 0.20$. The deformation in the composite plate is initially arrested as indicated by the smaller jump in displacement between $t = 400$ μs and $t = 600$ μs in comparison to the change in displacement between $t = 200$ μs and $t = 400$ μs. However, at $t = 800$ μs, the deforming laminate experiences cracking at the backface and a 45° crack travels from the backface to the frontface.

Comparing the computational results for the carbon-fiber laminate and glass-fiber laminate shows that the glass-fiber composite plate experiences significantly greater out-of-plane deflection for similar applied impulse. Since the tensile stresses created in a bending plate are strongly dependent on out-of-plane deflection, the glass-fiber laminate primarily undergoes damage and cracking at the midsection. Additionally, interlaminar damage, fracture, and separation are restricted to the region close to the center of the plate. Fig. 15 shows the experimental and computational out-of-plane

deflection histories for carbon-fiber/epoxy laminates with different layups. The quasi-isotropic laminate experiences the least deflection, followed by the biaxial laminate, laminate with fibers oriented perpendicular to supports, and parallel to supports, in that order. Initially, the rate of deformation for all plates is similar but as the deformation progresses. As deformation progresses, the quasi-isotropic and biaxial laminates experience a reduction in the rate of bending at $t = 800$ μs.

Laminates with fibers oriented parallel to the supports exhibit the least blast resistance, due to their inability to transmit the incident impulse to the supports and mitigate the effects of incident impulsive loads. The laminate with fibers oriented parallel to the supports undergoes the greatest deflection, with a normalized deflection (Δ/L) of 0.6. The laminate with fibers oriented perpendicular to supports undergoes 60%, the biaxial plate undergoes 50%, and the quasi-isotropic plate experiences 40% of the deflection experienced by the laminate with fibers oriented parallel to the supports. The computational model accounts for the essential aspects of deformation but the continuum damage framework underestimates the
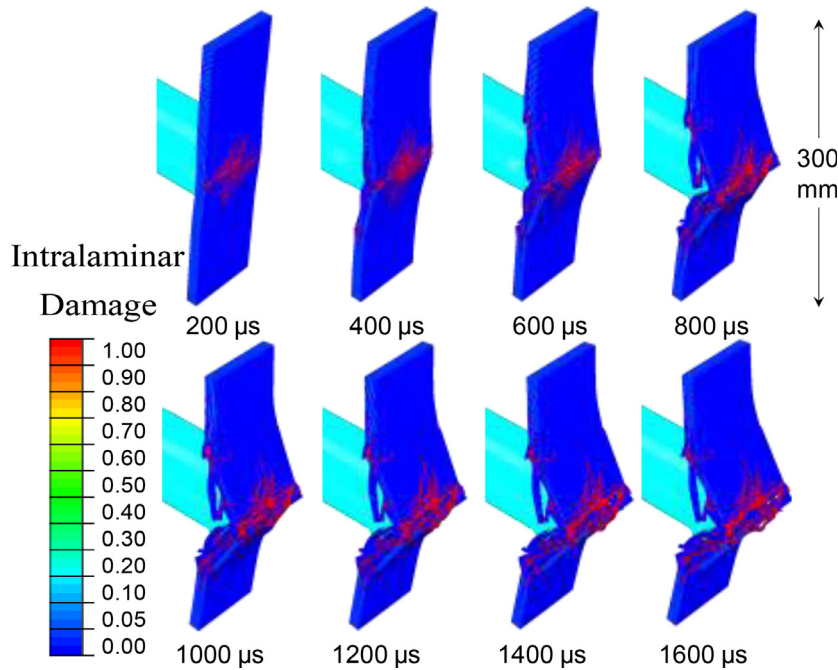
Fig. 14. Distributions of in-ply damage in a quasi-isotropic glass-fiber/epoxy composite laminate subjected to $\bar{I} = 0.20$.
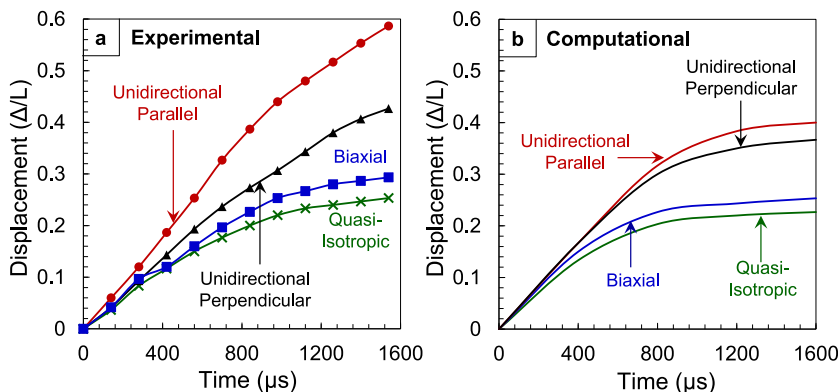
Fig. 15. Experimentally measured and numerically calculated midpoint displacements as functions of time for carbon-fiber/epoxy laminates to similar incident impulsive loads.

stiffness of the plate resulting in artificial softening which leads to a lower rate of deformation post-failure in comparison to the experiments. However, the model accurately captures the relative blast resistance of each composite laminate.

3.2. Out-of-plane deflection

The out-of-plane deflection histories of glass-fiber/epoxy laminates with different fiber layups are shown in Fig. 16. Glass-fibers are inherently more compliant, possessing approximately 30% of the stiffness and strength of carbon-fibers despite being 20% heavier by weight. This is reflected in the deflection of the glass-fiber/epoxy plates which show a clear softening behavior under water-based impulsive loading. The quasi-isotropic laminate experiences the least deflection, with a normalized deflection (Δ/L) of 0.35 with the biaxial plate experiencing 10% more deflection, the plate with fibers oriented parallel to supports experiencing 20% more deflection, and fiber oriented perpendicular to supports experiencing 40% more deflection. The rate of impulse transmission and the magnitude of the transmitted impulse can provide valuable insight into the blast resistance and performance of composite structures. Fig. 17(a) shows the reaction forces measured at the supports in finite element simulations while Fig. 17(b) shows the corresponding impulses calculated using $I = \int F \cdot dt$.

The Hashin damage model used in this computational approach consists of damage modes that encompass tensile matrix cracking, compressive matrix cracking, tensile fiber cracking and compressive matrix cracking. Since cracking initiates due to high tensile stresses caused by bending, the intralaminar damage considered for the purposes of damage quantification is the

tensile damage occurring in the matrix and fibers. A cohesive zone model is used to evaluate interlaminar cracking. Evaluating the rate and extent of damage can provide a deeper insight into the performance of each composite plate. In order to evaluate the total damage in impulsively loaded composite structures, we use a cumulative damage term called "accumulated damage" defined by $\overline{N}$ = Number of Failed Elements/Total Number of Elements.

Fig. 18(a) shows the ratio of the number of elements undergoing intralaminar damage and the total number of elements described by the Hashin damage model as a function of time for quasi-isotropic carbon-fiber/epoxy and glass-fiber/epoxy laminates subjected to $\bar{I} =$ 0.20. The glass-fiber/epoxy specimen experiences damage in ∼40% of the laminate while the carbon-fiber/epoxy specimen experiences damage in ∼10% of the laminate. Fig. 18(b) shows the ratio of the number of elements undergoing interlaminar damage and the total number of cohesive elements as a function of time for quasi-isotropic carbon-fiber/epoxy and glass-fiber/epoxy laminates subjected to $\bar{I} = 0.20$. The glass-fiber/epoxy specimen experiences damage in ∼60% of the interlaminar "resin-rich" regions while the carbon-fiber/epoxy specimen experiences damage in ∼10% of the interlaminar regions.

3.3. The effects of load obliquity on structural response

The different angle of incidence creates complicated loading conditions with the bottom portion of the composite experiencing the incident impulse prior to the upper portion. The uneven incident loading leads to two different regions of highly localized damage. Distributions of damage in an obliquely loaded monolithic composite plate with $\theta = 10°$ subjected to $\bar{I} = 0.20$ are shown in Fig. 19. The
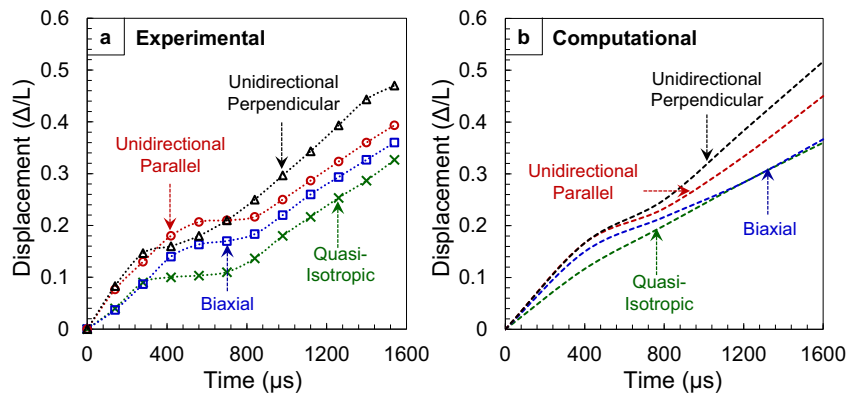
Fig. 16. Experimentally measured and numerically calculated midpoint displacements as functions of time for glass-fiber/epoxy laminates to similar incident impulsive loads.
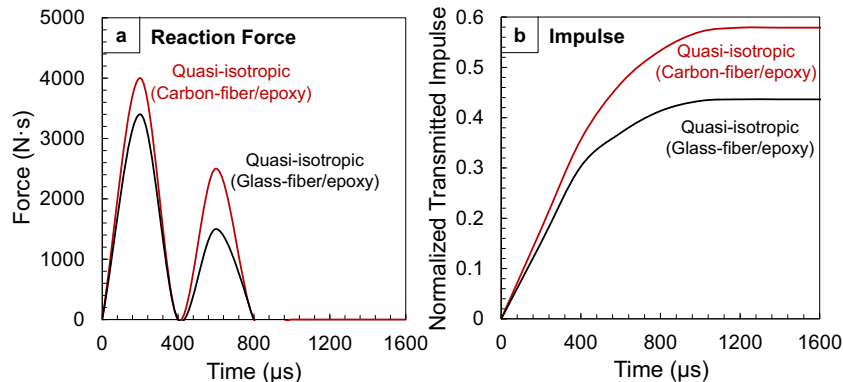
Fig. 17. Calculated reaction forces and transmitted impulses as functions of time for carbon-fiber/epoxy and glass-fiber/epoxy laminates subjected to similar incident impulsive loads.
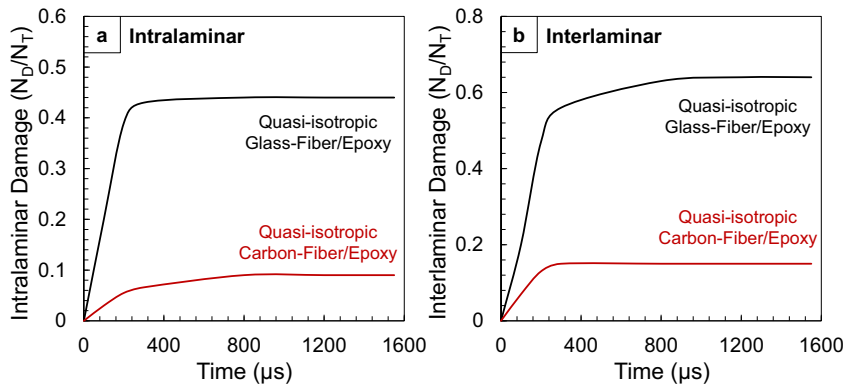
Fig. 18. Calculated reaction forces and transmitted impulses as functions of time for carbon-fiber/epoxy and glass-fiber/epoxy laminates subjected to similar incident impulsive loads.
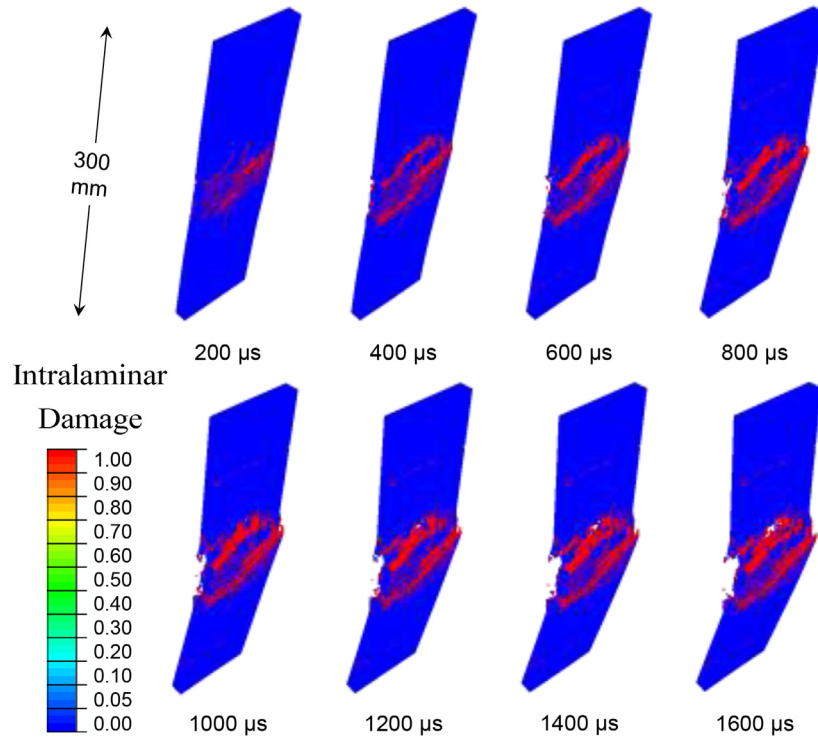
Fig. 19. Distributions of in-ply damage in an obliquely loaded quasi-isotropic carbon-fiber/epoxy composite laminate with $\theta = 10°$ subjected to $\bar{I} = 0.20$.

higher angle of obliquity creates multiple locations of localized damage and causes rupture near the upper supports. A comparison of deformation in planarly loaded plates shown in Fig. 9 and obliquely loaded plates in Fig. 19 indicates that higher angles of obliquity increase the number of locations in which localized deformation takes place.

Fig. 20 shows the out-of-plane displacement as a function of distance along the impulsively loaded plates at $t = 200, 400, 600, 800$ and 1000 μs. A major aspect of deformation in a simply-supported bending configuration is the formation of a highly stressed region near the center of the plate which experiences the highest out-of-plane deflection. However, results indicate that increasing angle of obliquity causes localized deformation to be triggered in multiple locations of the plate. The severity of the damage depends on the magnitude of obliquity. Higher obliquity causes an incident wave with the same magnitude to interact with a smaller area leading causing rupture in a localized region which propagates through the

rest of the plate. Fig. 21 shows the intralaminar and interlaminar damage in quasi-isotropic carbon-fiber/epoxy plates with different angles of obliquity subjected to $\bar{I} = 0.20$. Both interlaminar and intralaminar damage increase with increasing angles of obliquity. There is ~5% increase in damage for every 2° increase in the angle of obliquity.

4. Concluding remarks

Marine structures must balance stiffness and load-carrying capacity with the ability to minimize impulse transmission for high blast and impact resistance. Composite structures have higher stiffness and strength-to-weight ratios compared to metallic structures. Additionally, thick composite laminates provide very high bending and shear resistances with relatively small increases in total mass. However, due to the novelty and wide range of structural combinations, the relationships between structural responses and material
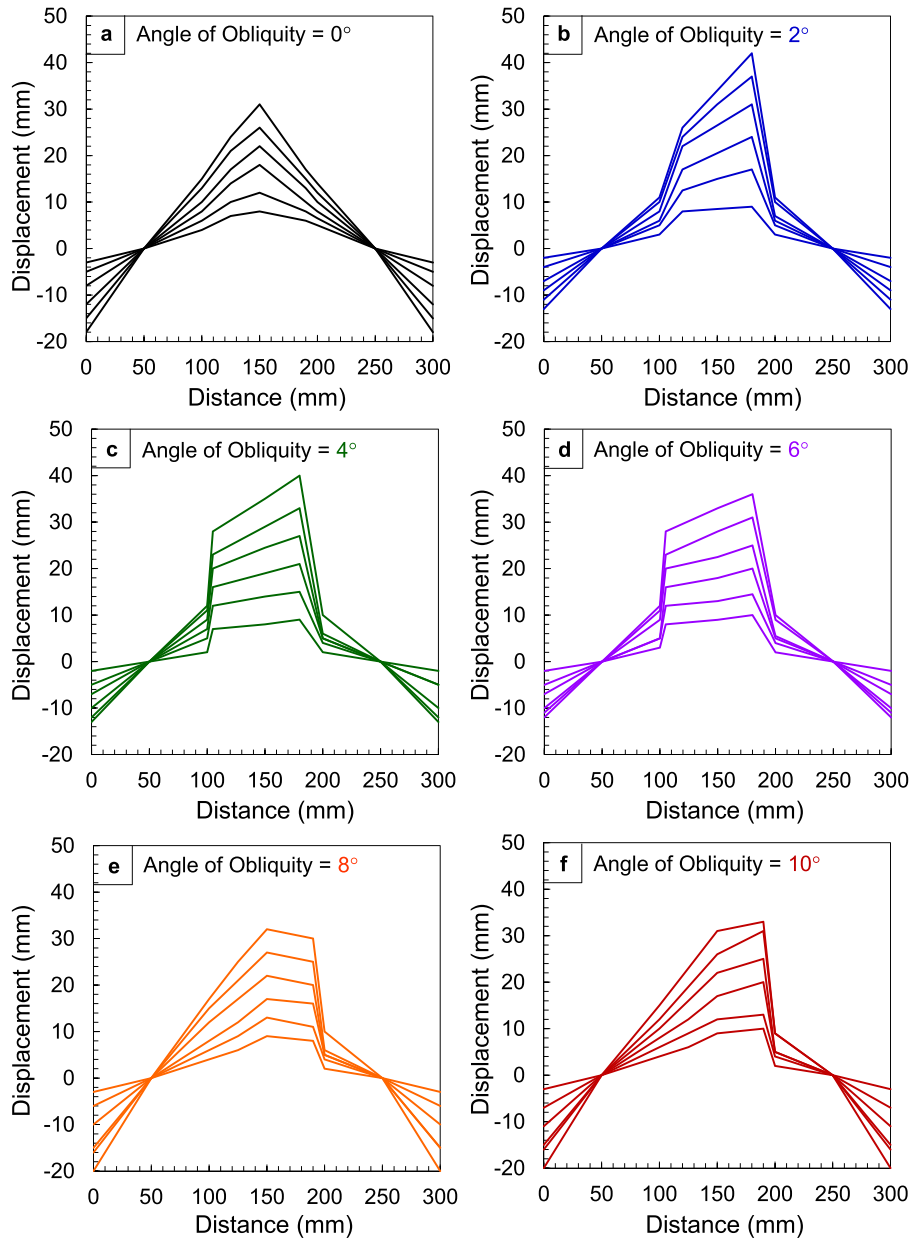
Fig. 20. Out-of-plane displacement as a function of distance at $t = 200, 400, 600, 800$ and $1000 \ \mu$s for composite laminates with different angles of oblique loading subjected to similar underwater impulsive loads.
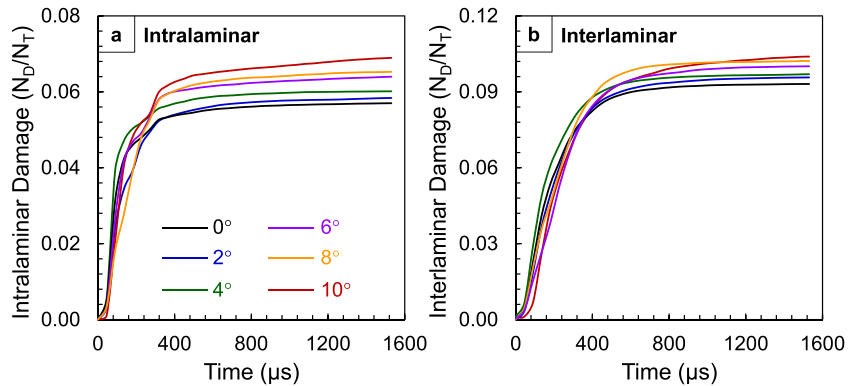
Fig. 21. Calculated damage histories for carbon-fiber/epoxy and glass-fiber/epoxy laminates subjected to similar underwater impulsive loads.

heterogeneity in composite structures are not well quantified. In particular, the behavior of composite structures under extreme impulsive loading generated by underwater explosions needs to be systematically analyzed. This research has been carried out to address this need.

The composite structures consist of both carbon-fiber and glass-fiber reinforced epoxy resin, and are manufactured by curing commercially available prepregs. The composites consist of 34% epoxy by weight, with the rest containing fibers. Four different composite layups are analyzed: (1) bi-axial; (2) quasi-isotropic; (3) unidirectional with fibers oriented parallel to supports; and (4) unidirectional with fibers oriented perpendicular to supports. It should be emphasized that the composite panels studied have quite similar in overall mass and thickness to enable comparison of performance. The combined experimental and computational research reported here focuses on the quantification of the water blast response of fiber-reinforced epoxy laminates with different material properties and stacking sequences under a range of incident impulsive loads. Since all plates experience failure under an incident impulse of $\bar{I} = 0.16$ with a peak pressure of 196 MPa, this is the highest impulse intensity discussed in this paper. The experiments reported here are supported by a fully dynamic three-dimensional computational framework which employs a Coupled Eulerian Lagrangian (CEL) approach to capture the effects of underwater blasts and fluid-structure interactions (FSI). The results from numerical calculations provide a more in-depth understanding of temporal and spatial evolution of different deformation modes in the structures and the damage mechanisms in different components.

Comparison of experiments and simulations shows that numerical calculations provide a reasonable representation of damage and dissipation mechanisms in the composite laminates. The finite element model captures the essential deformation mechanisms observed in both carbon-fiber and glass-fiber/epoxy laminates. Specifically, the following are replicated with reasonable accuracy: fluid-structure interaction effects at the water-structure interface, effects of fiber orientation, in-ply matrix and fiber cracking and rupture, and inter-ply delamination initiation and evolution. The Hashin damage model overestimates the softening effect resulting from cracking and fracture leading to a slight underestimation of backface deflection.

The unidirectional layups experience splitting due to a lack of stability in the transverse direction, while the bi-axial layups undergo failure near the loading circumference in close proximity to the impulsively loaded region. Quasi-isotropic layups provide the highest blast resistance for both the carbon-fiber and glass-fiber epoxy laminates. Additionally, the quasi-isotropic carbon-fiber/epoxy laminates experience 70% of the deflection experienced by glass-fiber/epoxy laminates. Since carbon-fiber laminates are nearly four times stiffer than glass-fiber laminates, it is expected that these laminates will transfer higher impulses due to more efficient load spreading. The impulse transmitted by the carbon-fiber laminates is ~130% of that transmitted by glass-fiber laminates, which is relatively modest increase in comparison to superior deflection resistance and reduced in-ply as well as inter-ply damage. In terms of accumulated damage, the carbon-fiber laminates experience 25% of the damage experience by glass-fiber laminates.

To evaluate the effects of load obliquity on the dynamic response of composite laminates, the loading angle is varied from 0° to 10° with increments of 2° and each loading configuration is subjected to similar incident loads. Results indicate that increasing angle of obliquity causes localized deformation to be triggered in multiple locations of the plate. Intralaminar damage increases with increasing angles of obliquity, while interlaminar damage is relatively insensitive to load obliquity. There is an ~5% increase in intralaminar damage for every 2° increase in the angle of obliquity.

References

[1] Chang FK, Choi HY, Jeng ST. Study on impact damage in laminated composites. Mech Mater 1990;10:83–95.
[2] Chang FK, Choi HY, Jeng ST. Characterization of impact damage in laminated composites. Sampe J 1990;26:18–25.
[3] Lessard LB, Chang FK. Damage tolerance of laminated composites containing an open hole and subjected to compressive loadings 0.2. Experiment. J Compos Mater 1991;25:44–64.
[4] Cantwell WJ, Morton J. The impact resistance of composite-materials - a review. Composites 1991;22:347–62.
[5] Hashin Z. Analysis of stiffness reduction of cracked cross-ply laminates. Eng Fract Mech 1986;25:771–8.
[6] Hashin Z. Analysis of orthogonally cracked laminates under tension. J Appl Mech-T Asme 1987;54:872–9.
[7] Minnaar K, Zhou M. A novel technique for time-resolved detection and tracking of interfacial and matrix fracture in layered materials. J Mech Phys Solids 2004;52:2771–99.
[8] Espinosa HD, Lee S, Moldovan N. A novel fluid structure interaction experiment to investigate deformation of structural elements subjected to impulsive loading. Exp Mech 2006;46:805–24.
[9] Latourte F, Gregoire D, Zenkert D, Wei XD, Espinosa HD. Failure mechanisms in composite panels subjected to underwater impulsive loads. J Mech Phys Solids 2011;59:1623–46.
[10] Wei XD, de Vaucorbeil A, Tran P, Espinosa HD. A new rate-dependent unidirectional composite model - Application to panels subjected to underwater blast. J Mech Phys Solids 2013;61:1305–18.
[11] Battley M, Allen T. Servo-hydraulic system for controlled velocity water impact of marine sandwich panels. Exp Mech 2012;52:95–106.
[12] Battley M, Stenius I, Breder J, Edinger S. Dynamic characterisation of marine sandwich structures. Sandwich structures7: advancing with sandwich structures and materials; 2005537–46.
[13] Tekalur SA, Bogdanovich AE, Shukla A. Shock loading response of sandwich panels with 3-D woven E-glass composite skins and stitched foam core. Compos Sci Technol 2009;69:736–53.
[14] Tekalur SA, Shukla A, Shivakumar K. Blast resistance of polyurea based layered composite materials. Compos Struct 2008;84:271–81.
[15] LeBlanc J, Shukla A, Rousseau C, Bogdanovich A. Shock loading of three-dimensional woven composite materials. Compos Struct 2007;79:344–55.
[16] Grogan J, Tekalur SA, Shukla A, Bogdanovich A, Coffelt RA. Ballistic resistance of 2D and 3D woven sandwich composites. J Sandwich Struct Mater 2007;9:283–302.
[17] Wang EH, Gardner N, Shukla A. The blast resistance of sandwich composites with stepwise graded cores. Int J Solids Struct 2009;46:3492–502.
[18] Avachat S, Zhou M. High-speed digital imaging and computational modeling of dynamic failure in composite structures subjected to underwater impulsive loads. Int J Impact Eng 2015;77:147–65.
[19] Schiffer A, Tagarielli VL. The one-dimensional response of a water-filled double hull to underwater blast: experiments and simulations. Int J Impact Eng 2014;63:177–87.
[20] Schiffer A, Tagarielli VL. The response of rigid plates to blast in deep water: fluid-structure interaction experiments. Proc R Soc A 2012;468:2807–28.
[21] Avachat S, Zhou M. Effect of facesheet thickness on dynamic response of composite sandwich plates to underwater impulsive loading. Exp Mech 2011;52:83–93.
[22] Avachat S, Zhou M. Dynamic response of composite sandwich structures subjected to underwater impulsive loads. In: Ferreira AJM, editor. Experiments and simulations conference proceedings of the 16th international conference on composite structures, ICCS-16. Porto: FEUP; 2011. 2011.
[23] Avachat S, Zhou M. Dynamic response of submerged composite sandwich structures to blast loading. In: Shukla Arun, editor. Proceedings of the IMPLAST 2010 - SEM fall conference, October 12-14 2010 Providence, Rhode Island, USA; 2010.
[24] Wei XD, Tran P, de Vaucorbeil A, Ramaswamy RB, Latourte F, Espinosa HD. Three-dimensional numerical modeling of composite panels subjected to underwater blast. J Mech Phys Solids 2013;61:1319–36.
[25] Swisdak MM. Explosion effects and properties: Part II – explosion effects in water, Dahlgren, Virginia, USA: Naval Surface Weapons Center Technical Report; 1978.

[26] Taylor GI. The pressure and impulse of submarine explosion waves on plates. The scientific papers of G I Taylor, vol. III. Cambridge: Cambridge University Press; 1941. p. 287–303.

[27] Arora H, Kelly M, Worley A, Del Linz P, Fergusson A, Hooper PA, et al. Compressive strength after blast of sandwich composite materials. Philos Trans R Soc A 2014;372.

[28] Arora H, Hooper PA, Dear JP. The effects of air and underwater blast on composite sandwich panels and tubular laminate structures. Exp Mech 2012;52:59–81.

[29] Taylor GI. The scientific papers of G I Taylor. Cambridge: Cambridge University Press; 1963.

[30] Kambouchev N, Radovitzky R, Noels L. Fluid-structure interaction effects in the dynamic response of free-standing plates to uniform shock loading. J Appl Mech 2007;74:1042–5.

[31] Hutchinson JW. Energy and momentum transfer in air shocks. J Appl Mech 2009;76.

[32] Hashin Z. Failure criteria for unidirectional fiber composites. J Appl Mech-T Asme 1980;47:329–34.

[33] Puck A, Schürmann H. Failure analysis of FRP laminates by means of physically based phenomenological models. Compos Sci Technol 1999;62(12−13):1633–62 September−October 2002.

[34] Schubel PM, Luo JJ, Daniel IM. Low velocity impact behavior of composite sandwich panels. Compos Part A 2005;36:1389–96.

[35] Kiel AH. The response of ships to underwater explosions. Department of the Navy; 1961.

[36] Chan S, Fawaz Z, Behdinan K, Amid R. Ballistic limit prediction using a numerical model with progressive damage capability. Compos Struct 2007;77:466–74.

[37] Pinho ST, Robinson P, Iannucci L. Fracture toughness of the tensile and compressive fibre failure modes in laminated composites. Compos Sci Technol 2006;66:2069–79.

[38] Lapczyk I, Hurtado JA. Progressive damage modeling in fiber-reinforced materials. Compos Part A 2007;38:2333–41.

[39] Needleman A. An analysis of tensile decohesion along an interface. J Mech Phys Solids 1990;38:289–324.

[40] Tvergaard V, Hutchinson JW. The relation between crack-growth resistance and fracture process parameters in elastic plastic solids. J Mech Phys Solids 1992;40:1377–97.

[41] Tvergaard V, Needleman A. Effect of crack meandering on dynamic, ductile fracture. J Mech Phys Solids 1992;40:447–71.

[42] Needleman A, Tvergaard V. Mesh effects in the analysis of dynamic ductile crack-growth. Eng Fract Mech 1994;47:75–91.

[43] Xu XP, Needleman A. Numerical simulations of fast crack-growth in brittle solids. J Mech Phys Solids 1994;42:1397.

[44] Camacho GT, Ortiz M. Computational modelling of impact damage in brittle materials. Int J Solids Struct 1996;33:2899–938.

[45] Espinosa HD, Zavattieri PD, Dwivedi SK. A finite deformation continuum discrete model for the description of fragmentation and damage in brittle materials. Pergamon: Elsevier Science Ltd; 1998. p. 1909–42.

[46] Camanho PP, Davila CG, de Moura MF. Numerical simulation of mixed-mode progressive delamination in composite materials. J Compos Mater 2003;37:1415–38.

[47] Minnaar K, Zhou M. Characterization of impact in composite laminates. AIP conference proceedings, 620; 2002. p. 1208.

[48] Zhai J, Zhou M. Finite element analysis of micromechanical failure modes in a heterogeneous ceramic material system. Int J Fract 2000;101:161–80.

[49] Gullerud AS, Gao XS, Dodds RH, Haj-Ali R. Simulation of ductile crack growth using computational cells: numerical aspects. Eng Fract Mech 2000;66:65–92.

[50] Tomar V, Zhai J, Zhou M. Bounds for element size in a variable stiffness cohesive finite element model. Int J Numer Methods Eng 2004;61:1894–920.